A Visual Analytics Approach to Diagnosis of Breast DCE-MRI Data

Sylvia Glaßer, Sebastian Schäfer, Steffen Oeltze, Uta Preim, Klaus D. Tönnies, Bernhard Preim

Department of Simulation and Graphics, Otto-von-Guericke University Magdeburg
Contact email: glasser@isg.cs.uni-magdeburg.de

Abstract

Dynamic contrast-enhanced magnetic resonance imaging (DCE-MRI) of the breast has become an important image modality for early breast cancer detection. In comparison to conventional X-ray mammography it exhibits a higher sensitivity, but only moderate specificity. To improve the specificity, and therefore the distinction of benign and malignant changes, the lesion's heterogeneity and the lesion enhancement kinetics have to be evaluated. We present a visual analytics approach for breast tumors in DCE-MRI data that divides a tumor in different regions with different perfusion characteristics by employing a region merging method. The resulting region-based representation allows for evaluation of the tumor's heterogeneity and the region-wise qualitative and quantitative evaluation of the enhancement kinetics. The analyses are combined with a glyph-based representation for a fast overview of the whole lesion. We tested our approach with seven well-chosen lesions and compared them to their histopathologic reports.

1 Introduction

In the western countries, breast cancer is the most frequent malignant disease in women. Dynamic contrast-enhanced magnetic resonance imaging (DCE-MRI) of the breast is currently the most sensitive modality for invasive breast cancer detection [1]. Breast perfusion DCE-MRI data exhibits a high spatial and low temporal resolution. In comparison to conventional X-ray mammography it may reveal yet undetected lesions and is therefore the image modality of choice for high-risk patients and suspicious lesions detected with X-ray.

A breast tumor leads to the formation of new vessels and/or the sprouting of existing capillaries, which is referred to as angiogenesis or neoangiogenesis [1]. In DCE-MRI, a contrast agent (CA) is intravenously injected and works as a tracer of perfusion. The angiogenetic activity of a lesion leads to CA accumulations and allows for breast cancer detection. On the one hand, these newly formed vessels yield an early CA enhancement and therefore a strong CA wash-in. On the other hand, the highly permeable vessels cause a rapid CA wash-out.

Since DCE-MRI is applied in high risk and unpredictable cases, but only has a moderate specificity compared to X-ray mammography [1], the distinction of benign and malignant lesions should be improved. For the accurate assessment of breast cancer, no standardized evaluation guidelines but two main evaluation criteria [2] exist:

- the morphology of the lesion, and
- the lesion enhancement kinetics.

We focus on the second criterion. The evaluation of the enhancement kinetics is carried out by the definition of a region of interest (ROI) and the analysis of the average signal intensity change over time of this ROI. For the exact ROI's size and placement, different recommendations exist. In general, it should be very small and avoid inclusion of necrotic or surrounding tissue, since this could distort the averaged enhancement kinetics [1]. The heterogeneity of tumor vascularization, the close neighborhood of necrotic and vital tumor tissue, and the subjectiveness of ROI placement harden the interpretation of the kinetics and may even result in unrevealed malignant tissue. For example, if a ROI covers malignant and benign tissue, the resulting average curve may indicate benignity.

We propose a region-based visual analytics approach for breast tumors in DCE-MRI data. Our region merging method automatically provides regions with similar perfusion characteristics. Quantitative analysis of the enhancement kinetics reveals the most suspicious region as well as the heterogeneity of the lesion. For qualitative analysis, the regions are analyzed in terms of perfusion parameters. The region-wise approach is combined with

a glyph-based voxel-wise representation of the lesion, which provides a fast overview of the CA accumulation in combination with its kinetics. We finally present a case study, containing different DCE-MRI tumor datasets together with histopathologic reports.

2 Related Work

A number of computer-aided detection and diagnosis techniques for breast cancer have been proposed in the last decade. Mostly, a preselection of voxels or a segmentation is created, as a basis for further analyses. Coto et al. [14] employ enhancement scatterplots of the precontrast intensity and relative enhancement to let the user select voxels of interest. Chen et al. [15] propose a fuzzy c-means algorithm followed by binarization and optimization steps to automatically segment tumors. The binarization leads to a classification in background and lesion for quantification purposes. Tönnies et al. [16] introduced region merging to segment dynamic nuclear image data of the heart based on a region's time activity.

For the visual exploration of DCE-MRI data, Behrens et al. [9] proposed some basic visualization techniques. A more advanced concept, the Profile Flag, was described by Mlejnek et al. [13], and allows for the intuitive probing and annotation of temporal data. The visualization of the temporal curves is closely connected to the rendering of the anatomic structure of the data without removing any parts thereof. Kohle et al. [11] presented a new approach for volume visualization of these datasets. A color mapping for the highlighting of perfusion abnormalities and the closest vessel projection to add depth information to maximum intensity projections are employed. Other approaches employ glyph-based visualizations for mapping several parameters in one image. In [10], a survey of the visual exploration and analysis of perfusion data is provided. Existing approaches are limited to certain samples, slices or parts of the dataset. In contrast, we aim at an region-based analysis of the lesion.

Hauth et al. [7] presented an DCE-MRI breast tumor analysis approach by employing the three-time-point method for curve classification [4, 5]. The curve course is mapped to color and the relative enhancement of the CA is mapped to intensity. Hauth et al. [7] recommended the evaluation of the whole lesion for taking the tumor's heterogeneity into account. Englmeier et al. [8] also employed a mapping of parameters to color and intensity, but the user has to infer the parameter value from the associated color and intensity component. Beyond the evaluation of the entire lesion, different approaches exist for analysing smaller parts of the lesion. To reduce variations, Mussurakis et al. [6] recommend at least three different ROIs per lesion. Recommendations for the optimal ROI size in breast cancer diagnosis range from 3-4 pixels to the whole enhancing lesion [1, 2, 6]. We will reduce distortion due to ROI averaging or subjective ROI placement with automatically defined regions.

3 Method

Our method comprises of two steps that are intended to gradually extract and visualize perfusion parameters of breast DCE-MRI data, and thus to reveal suspicious lesions. In the first step, the data is segmented such that a lesion is divided into one or more homogenous regions in terms of perfusion characteristics. In the second step, a glyph-based overview is generated and statistical analyses of inner-regional perfusion parameters are provided.

3.1 Image Data

We applied our approach to five DCE-MRI datasets, containing seven lesions. For each lesion, a histopathologic report was available. The datasets were acquired with a 1,5T MRI scanner and exhibit the parameters: in-plane resolution $\approx 0.67 \times 0.67 mm^2$, matrix$\approx 528 \times 528$, number of slices ≈ 100, slice gap = $1.5mm$, number of acquisitions $= 5 - 6$ and total acquisition time $\approx 400sec$.

3.2 Motion Correction and Perfusion Parameter Extraction

DCE-MRI data exhibit motion artifacts mainly due to thorax expansion through breathing and patient's movement. To establish a better inter-pixel correspondence and reduce the interference, motion correction is carried out. The motion correction was performed in Me*VisLab* (www.mevislab.de), employing the elastic registration method developed by Rueckert et al. [12].

To quantify the relative enhancement (RE) of a lesion, the percentaged signal intensity increase is calculated [2]:

$$RE = \frac{(SI_c - SI)}{SI} \times 100, \qquad (1)$$

where SI is the precontrast and SI_c is the postcontrast signal intensity. The RE can be plotted over time, yielding RE curves (REC), which can be classified into three different types [2]. Type I corresponds to a straight (Ia) or curved (Ib) continuously enhancing REC. Type II is a plateau curve and type III corresponds to an ascending wash-in phase followed by a descending wash-out phase, see Fig. 1. A type III REC is indicative for malignancy [2].

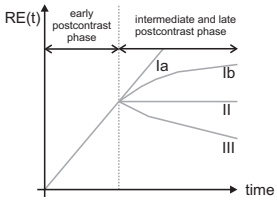

Figure 1: Schematic drawings of REC courses (reproduced from [2]). Type I corresponds to a straight (Ia) or curved (Ib) line. Type II is a plateau curve and type III a wash-out time course.

Beyond the classification of the REC course, the curves can be further characterized by descriptive perfusion parameters. We consider the following parameters, derived from the REC (see Fig. 2):

- Peak enhancement (*PE*). The maximum value of the REC.
- Time to peak (*TTP*). The point in time where *PE* occurs. Wash-in takes place between the first time point and *TTP*, whereas the wash-out occurs between *TTP* and the last time point.
- *Integral*. The approximated area under the REC for the whole time period.
- *UpSlope*. The curve's steepness during wash-in.
- *DownSlope*. The steepness of the descending curve during wash-out.

See [10] for further information about descriptive perfusion parameters.

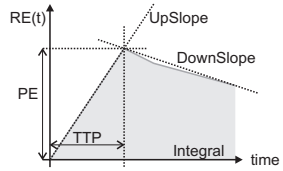

Figure 2: A REC with annotated perfusion parameters *PE*, *TTP*, *Integral*, *UpSlope* and *DownSlope*.

3.3 Segmentation

The evaluation of the lesion enhancement kinetics is carried out on the average REC of a certain ROI. Therefore, we provide a region merging segmentation for automatic ROI identification. The purpose of our approach is to create regions with similar perfusion characteristics to form ROIs. Hereby, noise is suppressed through averaging the voxel intensities in the regions and artifacts, i.e. motion or blurring, are not reinforced. Tumorous regions, exhibiting different perfusion characteristics, are kept apart in order to avoid that malignant tissue of a tumor is neglected because of surrounding benign tissue.

To speed up the segmentation and to avoid the processing of irrelevant regions, a preprocessing step is performed for background exclusion. There are two main indications for a voxel to be considered as background (and not as part of a lesion). First, the RE at the first time step after the early postcontrast phase is below a specified threshold T_{PE}, or second, the average RE change is below a certain threshold T_{CI} as a sign of non-perfused tissue, noise or artifacts. If a voxel's REC does not exceed one of these thresholds, it is set to background and not considered in the following. Note that voxels with a late enhancement will not be set to background, because of T_{CI}.

Subsequently, region-merging [17] is employed to arrange the voxels into regions. Initially, each voxel is a separate region. Iteratively, the most similar, adjacent regions are merged until the similarity of all regions falls below a pre-defined threshold or the number of regions is reduced to a pre-defined number. Regions are kept in a region adjacency graph. The similarity of adjacent regions is stored in a tree structure for a fast access (O(log n)) to the most similar pair of regions.

We investigated two different similarity criteria to compare two regions, each one characterized

by the average RE values of the contained voxels. The first one employs a priori knowledge regarding the characteristic perfusion parameters of the REC. Therefore, the average slope during early postcontrast phase (S_{early}) and the average slope during late postcontrast phase (S_{late}) of a region are calculated and, together with the region's peak enhancement $PE(R)$, regarded as a feature vector FV_1:

$$S_{early}(R) = \left(\frac{R_p - R_0}{R_0}\right) \quad (2)$$

$$S_{late}(R) = \left(\frac{R_p - R_{n-1}}{R_{n-1}}\right) \quad (3)$$

$$FV_1(R) = \begin{pmatrix} S_{early}(R) \\ S_{late}(R) \\ PE(R) \end{pmatrix}. \quad (4)$$

R_t denotes the average RE value of region R at time step t with n time steps in the dataset overall and p represents the first time point after the early postcontrast phase. The pearson correlation of the feature vectors of two regions is computed as a similarity measurement.

The second similarity criterion is designed to investigate the performance of the region merging without a priori knowledge. For the feature vector FV_2, the averaged RE of each region is employed:

$$FV_2(R) = (R_0, ..., R_{n-1})^T. \quad (5)$$

Again, the pearson correlation of the feature vectors is computed as a similarity measurement.

For both approaches, a correlation value from which on regions should be considered as similar, can be specified. If no more region pairs fulfilling this threshold can be found, the region merging terminates.

We compared the segmentation results generated by both similarity criteria merging regions with a correlation equal to or greater than 0.99. The regional inhomogeneity of each perfusion parameter, normalized by the ratio of mean and standard deviation, and the average number of voxels in each region are computed for the seven lesions of our study are depicted in Fig. 3. As expected, the parameter-based similarity criterion FV_1 leads to a lower regional inhomogeneity. In addition, the number of regions containing a higher number of voxels is smaller compared to the results of the second similarity criterion FV_2. Together with the increased homogeneity, the higher number of voxels leads to a better reliability and expressiveness of the regions.

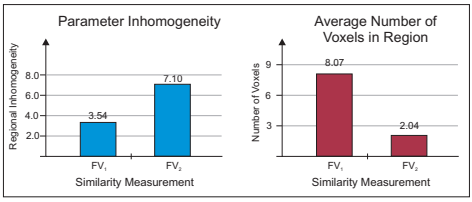

Figure 3: The charts evaluate the segmented regions of all seven lesions generated by applying the similarity criteria FV_1 and FV_2. The average inhomogeneity of the descriptive perfusion parameters, approximated with the mean and standard deviation ratio is shown in the left chart. The right chart shows the average number of voxels per region.

Therefore, we employ the perfusion parameter-based similarity criterion FV_1. Further analysis is only applied to regions with a minimum size S_{min}, i.e. at least 10 voxels or 1% of the lesion's size. S_{min} can be adapted by the user, depending on the level of detail the user is interested in. To separate the segmented lesion from the dataset, a one-click user interaction is necessary.

Since the influence of noise on small regions is higher than on regions containing a higher number of voxels, in theory, the correlation threshold should be adapted to account for this. We neglect this adaption, as our results indicate that regions of similar perfusion characteristics are found, and leave this to further investigation.

3.4 Visualization

We provide different approaches for the visualization of the lesion and the visual analyses of the segmentation result. First, we introduce a voxel-wise glyph-based overview for the simultaneous mapping of RE and curve courses. Second, we present quantitative and qualitative diagrams, for evaluation of the lesion's heterogeneity as well as for evaluation of the region-wise perfusion characteristics.

Glyph-based Overview Visualization

We developed a glyph-based visualization for voxel-wise mapping of the RE as well as the en-

hancement kinetics. The amount of RE at a certain point in time is color-coded by employing a HLS color scale, whereas the H component determines the hue of the color and the L and S component determines its lightness and saturation, respectively. We employ two tresholds: T_{down} for the minimum RE and T_{up} for the maximum RE value. For restriction to suspicious enhancement, we use $T_{down} = 60\%$ and $T_{up} = 250\%$ as default values according to [2]. Color coding of RE is carried out by assigning red to RE values $\geq T_{up}$, blue to values equal to T_{down} and negative linear interpolation in HLS color space in between (see Fig. 4). Voxels that exhibit values $< T_{down}$, are mapped to grey, whereas the brightness is proportional to the RE, thus providing context information. However, T_{down} and T_{up} can be adapted for visual analysis. For example, if the sensitivity shall be increased, T_{down} must be decreased.

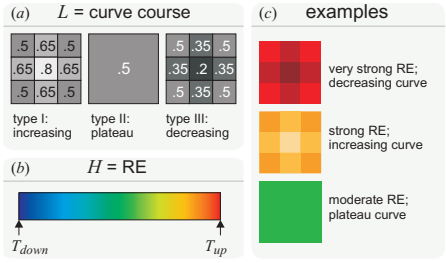

Figure 4: Voxel-wise mapping of RE and REC course to glyphs. The curve course determines the L component (a), whereas the RE value determines the hue of the glyphs (b). In (c), glyphs with different REC courses and RE values are presented.

The REC of each voxel is classified based on the three-time-point method [4, 5] for mapping of the enhancement kinetics. Therefore, a RE change in the intervall $\pm 10\%$ during wash-out will be interpreted as plateau, whereas RE changes higher than 10% and lower than -10% are considered as increasing and decreasing curve, respectively. Mapping of the REC course is realized by applying a 3×3 kernel for brightness modification. The S component of each glyph's color is assigned to 1, since we only use fully saturated colors for highlighting of the lesion's enhancement, see Fig. 5. In contrast to [7, 8] the RE and the REC course can be directly interpreted from the corners and the center of each glyph. Although the visualization is a little less intuitive, more information is provided, which may be important for special cases like a lesion with moderate enhancement but type III curves.

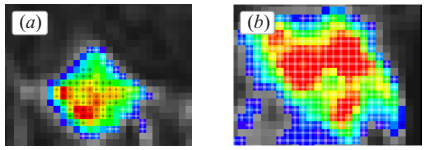

Figure 5: Glyph-based visualization of two lesions. In (a), malignancy is indicated, since in the lower left, there is a strong wash-in (red colors) and wash-out (type III courses, see darker centers of glyphs). In (b), a benign lesion with high RE values (red colors) and mostly type I and II curves (see brighter centers of glyphs) is depicted.

Region-based Quantitative Analysis

For quantitative analysis of the segmentation result, we provide information of the average RECs in the REC diagram. The segmentation yields n regions R_i (i=1..n) and the whole lesion L as the combination of these regions. In Fig. 6, the average REC of L and its regions R_i is depicted as well as the size of L and the percentaged size of each R_i. Type III RECs are highlighted with an increased line width. On the contrary, the line width could also be adapted to a region's reliability, which is region-wise approximated with the perfusion parameters' standard deviation in relation to the lesion. The REC diagram is linked with an interactive slice view, whereas each region is color coded according to the average REC diagram. The diagram is only applied to regions with a minimum size S_{min}. Regions can be selected and presented in the glyph-based visualization for further investigation, since the segmentation may yield regions with different curve types and RE values.

Parameter-based Qualitative Analysis

In addition to the quantitative evaluation of the REC diagram, we provide a statistical evaluation and thus the average μ_i of the descriptive perfusion parameters P_j, (j = *PE*, *TTP*, *Integral*, *UpSlope*, *DownSlope*) of each region R_i. The parameters *PE*, *Up-*

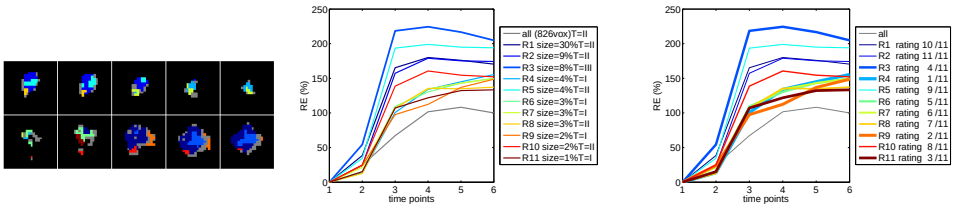

Figure 6: Representative slices of the lesion (left). Voxels that belong to smaller regions are mapped to grey. For larger regions, an average REC is created. The average REC of the overall lesion (grey course) indicates a type II curve. The most suspicious region R_3 is classified as type III and an increased line width is assigned (middle). The line width can also be adapted to the region's reliability (right).

Slope and *Integral* allow for the qualitative evaluation of the wash-in, whereas *DownSlope* and *TTP* are considered for the evaluation of the wash-out phase.

Beyond the numerical results, a qualitative region-wise analysis of the enhancement kinetics is provided. For a fast overview and visual distinction we establish the measure C_{i_j}, which characterizes the percentaged change of the average $\mu_i\,(P_j)$ for each region R_i and each parameter P_j, in comparison to the average perfusion parameter value $\mu_L\,(P_j)$ of the whole lesion L.

Since the parameters *PE* and *Integral* describe the wash-in and thus a certain amount of CA accumulation, they are considered as quantitative descriptors. We use the relative amount of change (see Eq. (6)), since the comparison should indicate trends instead of providing absolute differences of these descriptors. *UpSlope* and *DownSlope* are derived from the same REC and can be simply compared by difference (see Eq. (7)). *TTP* describes the point in time where *PE* is achieved. Since breast DCE-MRI datasets typically contain $5-6$ time points, we normalize the difference of L and region R_j with t_n, the number of time points (see Eq. (8)).

Calculation of C_{i_j} (i=1..n) for j = *PE, Integral*:

$$C_{i_j} = \frac{\mu_i(P_j) - \mu_L(P_j)}{\mu_L(P_j)} * 100, \qquad (6)$$

for j = *UpSlope, DownSlope*:

$$C_{i_j} = \mu_i(P_j) - \mu_L(P_j), \qquad (7)$$

and for j = *TTP*:

$$C_{i_j} = \frac{\mu_i(P_j) - \mu_L(P_i)}{t_n} * 100. \qquad (8)$$

In Fig. 7, the change diagram containing the changes C_{i_j} for each P_j is depicted (color coding is synchronized with the REC diagram). In conclusion of Eq. (6)-(8), the values of $\mu_L\,(P_j)$ are placed at zero along the abscissa. Different perfusion characteristics of a region in comparison to L are indicated by higher bars (considering the absolute height), whereas similar characteristics are indicated by smaller bars (considering the absolute height). In Fig. 7, the regions R_1, R_2, R_3 and R_5 indicate suspicious enhancement kinetics, since they exhibit a stronger wash-in (in terms of parameters *PE, Integral, UpSlope*) and a stronger wash-out (high negative magnitudes for *DownSlope, TTP*) in comparison to the whole lesion.

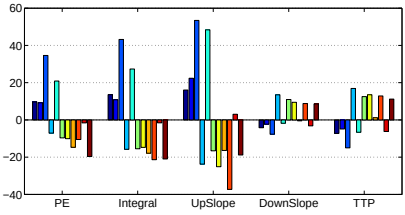

Figure 7: The change diagram of the lesion presented in Fig. 5(a) and 6. The regions $R_1 - R_3$ and R_5 are very suspicious, because of the stronger wash-in (higher bars for *PE, Integral, UpSlope*) and a stronger wash-out (high magnitude for *DownSlope, TTP*) in comparison to the whole lesion.

4 Case Study

We present a case study which contains different malignant and benign lesions and their histopathologic reports, listed in Tab. 1. For each lesion, the results have been approved by a clinical expert. In this section, the result for each lesion is presented. In Fig. 8, representative slices with the glyph-based visualization, the REC and the change diagram of the lesions L_2 - L_7 are provided. Visualizations for L_1 were already presented in Fig. 5(a), 6 and 7.

Table 1: Listing of all lesions and histopathologic reports.

lesion	histopathologic report
L_1	malignant multicentric, invasive lobular carcinoma
L_2	benign lesion
L_3	malignant moderate differentiated invasive lobular carcinoma, contains small lobular carcinoma in situ
L_4	malignant moderate differentiated invasive ductal carcinoma
L_5	malignant inflammatory cancer
L_6	malignant mucinous carcinoma, contains benign fibroadenom
L_7	benign lesion with fibroadenoms

Lesion 1

The segmentation result for L_1 contains 826 voxels and 11 main regions. The glyph-based overview (see Fig. 5(a)) indicates malignancy with strong RE and type III RECs. Fig. 6 reveals a multicentric lesion. In the REC diagram, the largest region R_3 is classified as type III. Five regions with a type II REC exist and a strong heterogeneity can be observed. By analyzing the change diagram in Fig. 7, R_3 contains a strong wash-in (maximum *PE, Integral, UpSlope*) and wash-out (higher negative magnitude for *DownSlope* and earlier *TTP*) in comparison to the whole lesion. In combination with the type III REC, R_3 is highly suspicious and indicates malignancy. Moreover, the change diagram reveals suspicious type II regions R_1, R_2 and R_5 which exhibit similar attributes to R_3 in comparison to the whole lesion. The suspicion of malignancy is confirmed with the histophatologic report of L_1.

Lesion 2

The segmentation result contains a big lesion with 1311 voxels and eight regions. The glyph-based overview indicates continuous enhancement for many voxels. All regions exhibit a type I REC. The change diagram reveals that the regions differ in terms of *PE*, *Integral* and *UpSlope*, which is caused by different amounts of CA wash-in. They do not differ in terms of wash-out, since there are very small changes for *TTP* and *DownSlope*. No suspicious regions exist, indicating a benign lesion, which is confirmed by the report in Tab. 1.

Lesion 3

The segmentation yields a small lesion with 330 voxels and five regions. The glyph-based overview reveals suspicious enhancement kinetics for R_1. R_1, with a size of 50% and of type III, indicates malignancy, whereas other regions are continuously enhancing. The change diagram indicates similar perfusion characteristics of R_2-R_5 and strengthens the suspicion of R_1, since R_1 exhibits the strongest wash-out. The indications are confirmed with the report in Tab. 1.

Lesion 4

The segmentation contains a lesion with 710 voxels and nine regions. Although the glyph-based visualization reveals voxels with suspicious wash-in and wash-out kinetics, almost all regions are classified as type I in the REC diagram. Furthermore, only moderate RE (up to 160%) can be observed. The largest region R_1 is classified as type II. The change diagram shows the lesion's heterogeneity with different lesion enhancement kinetics. Especially the wash-out characteristics confirm R_1 as suspicious region, since it strongly differs from the other regions as well as the whole lesion. Although no type III curve exists, heterogeneity and wash-out indicate malignancy, which is confirmed by the report.

Lesion 5

The glyph-based overview reveals an inflammatory lesion with irregular contours, indicating inflammatory breast cancer. The segmentation for this specific cancer yields a huge (more than 120.000 voxels), highly fragmented lesion. The largest region R_1 contains only 16% of the lesion's voxels,

since many very small regions exist. The REC and change diagram exhibit heterogenous regions and many type III RECs. The indication of malignancy is confirmed in Tab. 1.

Lesion 6

For L_6, the segmentation leads to a large (4522 voxels), highly fragmented lesion. The glyph-based overview indicates moderate enhancement, with some small areas containing suspicious curve courses. The REC diagram does not reveal type III RECs, but it exhibits a strong heterogeneity. Furthermore, R_2 and R_4 are classified as type II. The change diagram illustrates the lesion's heterogeneity and suspicious perfusion parameter values of R_2 and R_4. Both regions strongly differ from the whole lesion, thus indicating malignancy. The suspect is confirmed by the histopathologic report. L_6 does contain smaller benign lesions, which may have caused regions with type I courses.

Lesion 7

The segmentation as well as the glyph-based overview yield a small, enhancing lesion (290 voxels) containing only three regions. Two are continuously enhancing and one ($R3$) is characterized by a plateau. R_3 has a strong RE (up to 300%) but does not exhibit any significant wash-out characteristic. This is strengthened by the change diagram, which reveals strong differences during wash-in (in terms of *PE*, *Integral*, *UpSlope*), but almost no differences during wash-out. The non-existence of characteristic wash-out kinetics indicates a benign lesion, which is confirmed in Tab. 1.

5 Results

In this section the results are summarized.

For background exclusion and voxel preselection described in Section 3.3, we employed a T_{PE} of 60% to select suspicious lesions [2]. T_{CI} was empirically set to 80%, since experiments revealed that this value allows for inclusion of regions with late enhancement. Segmentation results were generated with a correlation value of 0.99, up to which regions should be merged and considered as similar.

The segmentation results yield dense accumulations of small regions in peripheral parts of a lesion (see grey voxels in Fig. 8). If a region exhibits very similar curve parameters and a curve course with inferior signal intensities in relation to another region, it is most likely influenced by blurring, e.g. R_4, R_3 and R_8 of L_4. Motion artifacts may cause uncorrelated curve parameters of average RECs of adjacent inner-part regions, e.g. for L_4 in Fig. 8. In both cases, the signal is distorted and the corresponding regions should be considered as unreliable. Vice versa, bigger regions, in the inner-part of a lesion, do not include conspicuously impaired voxels. The segmentation process takes about 1 to 5 minutes for normal-sized lesions on a Pentium 4 (3,06 GHz) platform. The inflammatory lesion L_5 takes about 20 minutes.

The case study reveals the potential of the region-based analysis of perfusion parameters. In general, the glyph-based voxel-wise overview as well as the region-wise quantitative and qualitative evaluation with the REC and the change diagram provide additional information about the lesion enhancement kinetics and thus its malignancy.

Problems occur in special cases like a supplying vessel of a lesion. For L_4, parts of a vessel are contained in R_1. Since the vessel's enhancement kinetics are similar to parts of the lesion, the vessel is merged with R_1, resulting in an increased size of R_1. If a lesion exhibits heterogeneity but no region classified as type III (e.g. L_4 and L_6), the clinical expert can examine regions with type II RECs in more detail. Most important, the manual placement of ROIs could be constrained to a preselected, suspicious region. Thus, the clinical expert is supported and distortion due to averaging is avoided. Since all histopathologic reports were extracted after surgical intervention to clarify the clinical suspect of malignancy, our approach could increase specificity of lesion enhancement and might have avoided the interventions for benign lesions.

6 Conclusion and Future Work

We provide an approach for extraction and visual analysis of regions with similar perfusion characteristics. We described a case study of that approach, which indicates an improvement of specificity of tumor diagnosis in breast DCE-MRI. The region merging segmentation allows for improved perfusion analysis, since regions were merged based on similar perfusion characteristics. Furthermore, regions at the lesion's boundary, which exhibit en-

hancement variations due to noise or motion artifacts, could be excluded.

The glyph-based overview enables a voxel-wise and simultaneous evaluation of RE and curve courses. More sophisticated analyses, including visualizations of average RECs and curve classifications as well as perfusion characteristics in comparison to the whole lesion, allow for a region-wise evaluation and thus the lesion's heterogeneity and the identification of the most suspicious region. The most supicious region is essential for further diagnosis and treatment. The clinical expert's manual ROI placement can be constrained to this region.

For future work, the segmentation could be extended to automatically classify regions as impaired or reliable by analysing the RECs of adjacent regions. Adequate visualization techniques should be developed to represent this information.

Acknowledgements

This work was supported by the DFG Priority Program 1335: Scalable Visual Analytics. We thank Fraunhofer MEVIS for providing advanced MeVisLab features and Anja Hennemuth as well as Dr. Hendrik Laue for fruitful discussions.

References

[1] C. K. Kuhl. The Current Status of Breast MR Imaging, Part I. *Radiology,* 244(2):356–378, 2007.

[2] C. K. Kuhl, P. Mielcareck, S. Klaschik and et al. Dynamic Breast MR Imaging: Are Signal Intensity Time Course Data Useful for Differential Diagnosis of Enhancing Lesions? *Radiology,* 211(1):101–110, 1999.

[3] T. C. Williams, W. B. DeMartini, S. C. Partridge and et al. Breast MR Imaging: Computer-aided Evaluation Program for Discriminating Benign from Malignant Lesions. *Radiology,* 244(1):94–103, 2007.

[4] E. Furman-Haran, D. Grobgeld, F. Kelcz and H. Degani Critical role of spatial resolution in dynamic contrast-enhanced breast MRI. *J Magn Reson Imaging,* 13:862–867, 2001.

[5] H. Degani, V. Gusis, D. Weinstein and et al. Mapping pathophysiological features of breast tumors by MRI at high spatial resolution. *Nat Med,* 3:780–782, 1997.

[6] S. Mussurakis, D. L. Buckley and A. Horsman Dynamic MRI of invasive breast cancer: assessment of three region-of-interest analysis methods. *J Comput Assist Tomogr,* 21:431–438, 1997.

[7] E. A. Hauth, C. Stockamp, S. Maderwald and et al. Evaluation of the three-time-point method for diagnosis of breast lesions in contrast-enhanced MR mammography. *J Clinical Imaging,* 30(3):160–165, 2006.

[8] K. H. Englmeier and G. Hellwig and J. Griebel and et al. Morpho-functional visualization of dynamic MR-mammography. *Stud Health Technol Inform.* 107(2):838–841, 2004.

[9] U. Behrens, J. Teubner, C. Evertsz and et al. Computer-Assisted Dynamic Evaluation of Contrast-Enhanced-MRI. In *Proc. of CARS,* 362–367, 1996.

[10] B. Preim, S. Oeltze, M. Mlejnek and et al. Survey of the Visual Exploration and Analysis of Perfusion Data. In *IEEE Trans. on Visualization and Computer Graphics,* 15(2):205–20, 2009.

[11] S. Kohle, B. Preim, J. Wiener and et al. Exploration of time-varying data for Medical Diagnosis. In *Proc. of VMV,* pages 31–38, 2002.

[12] D. Rueckert, L. Sonoda, C. Hayes and et al. Nonrigid Registration Using Free-Form Deformations: Application to Breast MR Images In *IEEE Trans. Med. Imaging,* 18(8):712–721, 1999.

[13] M. Mjelnek, P. Ermes, A. Vilanova and et al. Application-Oriented Extensions of Profile Flags In *Proc. of EuroVis,* 339–346, 2006.

[14] E. Coto, S. Grimm, S. Bruckner and et al. MammoExplorer: An advanced CAD application for breast DCE-MRI. In *Proc. of VMV,* 91–98, 2005.

[15] W. Chen, M. L. Giger and U. Bick. A Fuzzy C-Means (FCM)-Based Approach for Computerized Segmentation of Breast Lesions in Dynamic Contrast-Enhanced MR Images. *Academic Radiology,* 13(1): 63–72, 2006.

[16] K.D. Toennies, A. Celler, S. Blinder and et al. Scatter segmentation in dynamic SPECT images using principal component analysis. In *Proc. of SPIE,* 2003.

[17] R.C. Gonzales and R.E. Woods. Digital Image Processing, *Prentice Hall,* 2002.

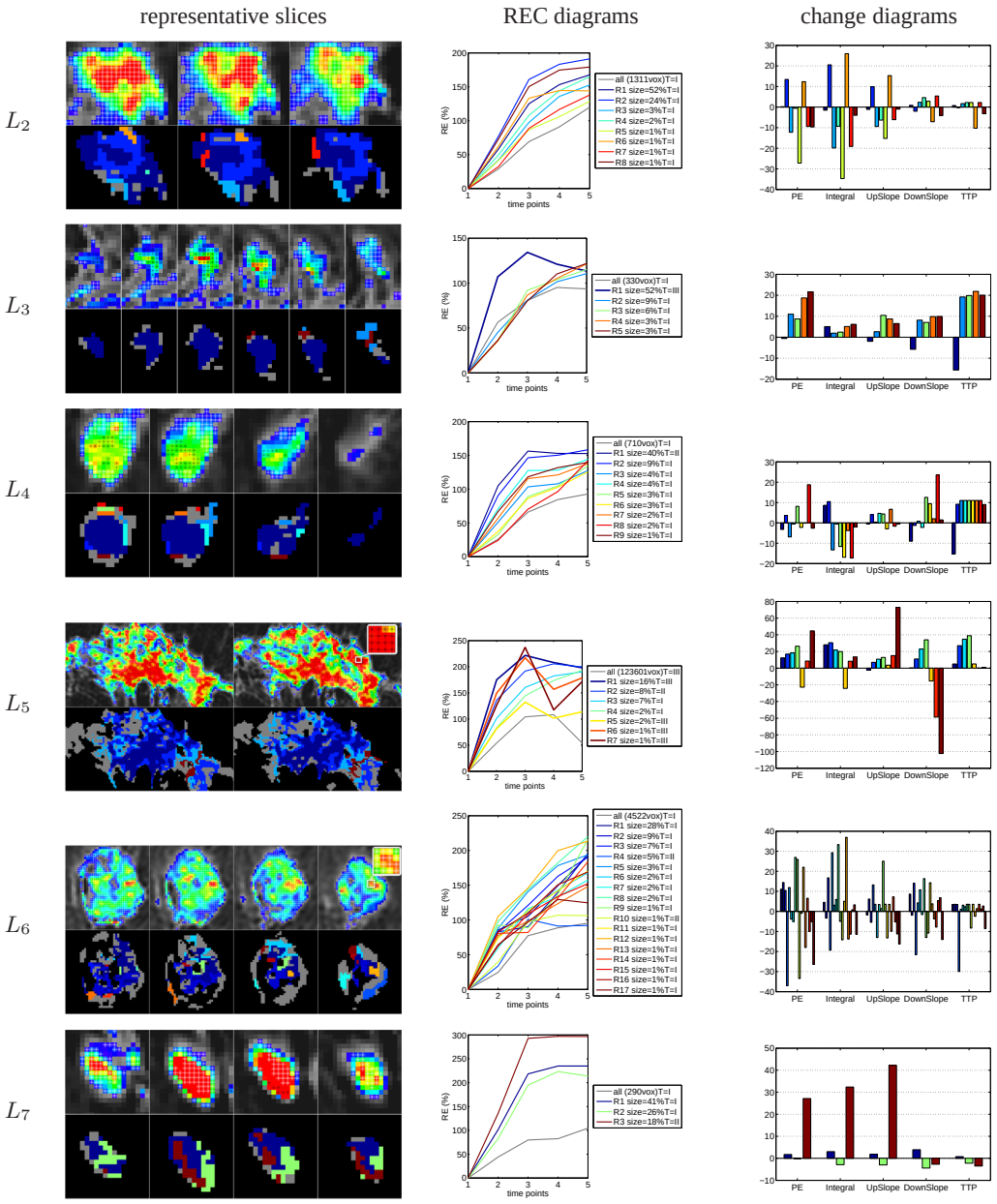

Figure 8: Evaluation results for each lesion L_2 - L_7. A glyph-based overview and a color coding of the regions for representative slices (left), as well as the REC diagram (center) and the change diagram (right) are provided. For the larger lesions L_5 and L_6, zooming is necessary for glyph interpretation.